

Principal Component Analysis of PSF Variation in Weak Lensing Surveys

Mike Jarvis, Bhuvnesh Jain

Dept. of Physics and Astronomy, University of Pennsylvania, Philadelphia, PA 19104

`mjarvis, bjain@physics.upenn.edu`

ABSTRACT

We introduce a new algorithm for interpolating measurements of the point-spread function (PSF) using stars from many exposures. The principal components of the variation in the PSF pattern from multiple exposures are used to solve for better fits for each individual exposure. These improved fits are then used to correct the weak lensing shapes. Since we expect some degree of correlation in the PSF anisotropy across exposures, using information from stars in all exposures leads to a significant gain in the accuracy of the estimated PSF. It means that in general, the accuracy of PSF reconstruction is limited not by the number density of stars per exposure, but by the stacked number density across all exposures in a given survey. This technique is applied to the 75 square degree CTIO lensing survey, and we find that the PSF variation is well described by a small number of components. There is a significant improvement in the lensing measurements: the residual stellar PSF correlations are reduced by several orders of magnitude, and the measured B-mode in the two-point correlation is consistent with zero down to 1 arcminute. We also discuss the applications of the PCA technique to future surveys.

Subject headings: gravitational lensing; cosmology; large-scale structure

1. Introduction

There are quite a few different systematic errors which can contaminate a weak lensing signal at the level of typical cosmic shear measurements. The largest of these has been the corrections of the anisotropic point-spread-function (PSF). Stars, which probe the PSF, are seen to have significantly elliptical shapes. Furthermore, on large cameras, the PSF can vary substantially across the image. Since the galaxy shapes are convolved by the PSF before you observe them, the effects of the PSF must be removed before performing any weak lensing analysis.

A number of techniques for removing the effects of the PSF have been proposed (Kaiser, Squires, & Broadhurst 1995; Hoekstra *et al.* 1998; Kaiser 2000; Bernstein & Jarvis 2002; Refregier & Bacon 2003). Recent lensing measurements (Van Waerbeke *et al.* 2002; Hoekstra *et al.* 2002; Refregier *et al.* 2002; Bacon *et al.* 2003; Brown *et al.* 2003; Hamana *et al.* 2003; Jarvis *et al.* 2003) have implemented these techniques well enough that the systematic errors are generally somewhat smaller than the statistical errors. However,

as the size of weak lensing surveys increases and the statistical errors keep going down, it becomes more important to similarly reduce the systematic errors.

This paper addresses the particular difficulty of interpolating the PSF between the stars in the image. Typically, the procedure has been to fit the various components of the PSF shape (the ellipticity, size, and possibly higher order components) to a polynomial function across the image. This technique is limited to probing variations in the PSF pattern which vary more slowly than the typical spacing between the stars. In fact it is somewhat worse than this, since the stellar shape measurements are often noisy, and there may be small galaxies masquerading as stars which have shapes which do not represent the PSF. Therefore, a smoother function with outlier rejection is required.

To address this problem, Hoekstra (2004) uses dense stellar fields to measure the high-order component of the PSF pattern, and then uses the stars in the individual images for a low-order correction to this pattern. This works well when the PSF pattern is reasonably stable so that the dense fields give a good first estimate of the pattern. However, in general, and for our data in particular (see §3), this will not be the case. Van Waerbeke, Mellier, & Hoekstra (2004) get better interpolation results when they switch from polynomials to rational functions. Rational functions are almost always better at modeling complicated functions, so they do a better job of modeling the PSF variation.

However, both of these methods do leave some residual B-mode contamination (see §3.3 for a discussion of the B-mode), indicating that there is still some uncorrected PSF anisotropy in the data. The residual is predominantly at small scales where high-order wiggles in the PSF pattern are not well modeled. In fact, it has been suggested that this level of B-mode may be an irreducible systematic for ground-based cosmic shear measurements, since there are simply too few stars to model the real PSF variation on these scales.

While it is likely true that there is some irreducible systematic effect on small scales, we show in this paper that it is much smaller than the previous results have indicated. The PSF pattern is found to be largely a function of only a few variables. Therefore, we are able to improve the fits of this pattern by using stars from many exposures. The limits to how well the PSF can be modeled are therefore governed not by the number of stars in a single exposure, but rather by the total number of stars from all of the exposures available.

In §2 we briefly review our CTIO survey data, largely deferring to Jarvis *et al.* (2003) for more details. We describe our new PSF modeling algorithm in §3 and conclude in §4.

2. Data

Our CTIO survey data was originally described in detail in Jarvis *et al.* (2003), and we refer the reader to that paper for the details about the data and the analysis. Here, we present merely a brief summary of the data set, and point out two changes from our previous analysis - the dilution correction and the PSF interpolation.

We observed 12 fields, well separated on the sky, each approximately 2.5 degrees on a side, giving us a total of 75 square degrees. We have useful galaxies for weak lensing in the magnitude range $19 < R < 23$,

which gives about 2 million galaxies to use for our lensing statistics.

The shape measurements of the galaxies follow the techniques of Bernstein & Jarvis (2002) using the convolution kernel method described therein. The first change from our previous analysis involves the dilution correction. Hirata & Seljak (2003) point out that our formula for the dilution was incorrect with respect to the kurtosis of the PSF. For the present analysis, we have incorporated their linear PSF correction which is described in Appendix B of their paper.

The second change we made is in the PSF interpolation. Since the convolution kernel is only measured where we have an observed star, and the PSF is far from uniform across each image, we need to interpolate between the stars. In our previous analysis, we used a separate fit for every image. For this analysis, however, we use our new PCA technique which is described in §3.

Finally, we estimate the shear, γ , from an ensemble of ellipticities using the “easy” weighting given in Bernstein & Jarvis (2002), equation 5.36, and using the corresponding responsivity formulae.

3. PCA Analysis of PSF fitting

It was clear from our previous analysis that the pattern of the PSF variation is not generally a simple function. In our previous analysis, we had found that fourth order polynomials were insufficient to fully describe the pattern. Unfortunately, with only a hundred or so stars per image, many of which are noisy and/or outliers, the data did not well constrain fits to higher order than this. We had slightly improved upon this by using a smoothing spline function, but that also failed to fully describe the variation.

This section describes our new technique of using Principal Component Analysis (PCA) to allow us to use all of the stars in every image to make a global fit of the PSF variation. This allows us to fit to a higher order polynomial in x and y , which seems to describe essentially all of the real variation of the PSF.

Figure 1 shows before and after “whisker plots” for three of our exposures. These exposures were taken with the Big Throughput Camera (BTC), for which the PSF patterns were significantly worse than with the Mosaic camera.¹ Each line (“whisker”) represents the ellipticity of an observed star. The length of the line is proportional to the ellipticity, and the orientation is the same as that of the star. The top row shows the plots for the three exposures before any corrections. The leftmost plot represents the most out of focus image in one direction, and the rightmost represents the extreme in the other direction.² The middle plot is far more typical, but apparently the four chips are not precisely coplanar, so they do not all come into focus at exactly the same time. The bottom row are the stars from the same three images after our corrections.

We note that observing a dense stellar field, as proposed by Hoekstra (2004), is not sufficient for our survey, since the PSF pattern changes dramatically with the relative focus position. Using the high order fit

¹Our entire survey includes approximately equal area of coverage for the two cameras.

²Specifically, these images have the largest and smallest $U(i, 1)$ value, which we describe in §3.1.

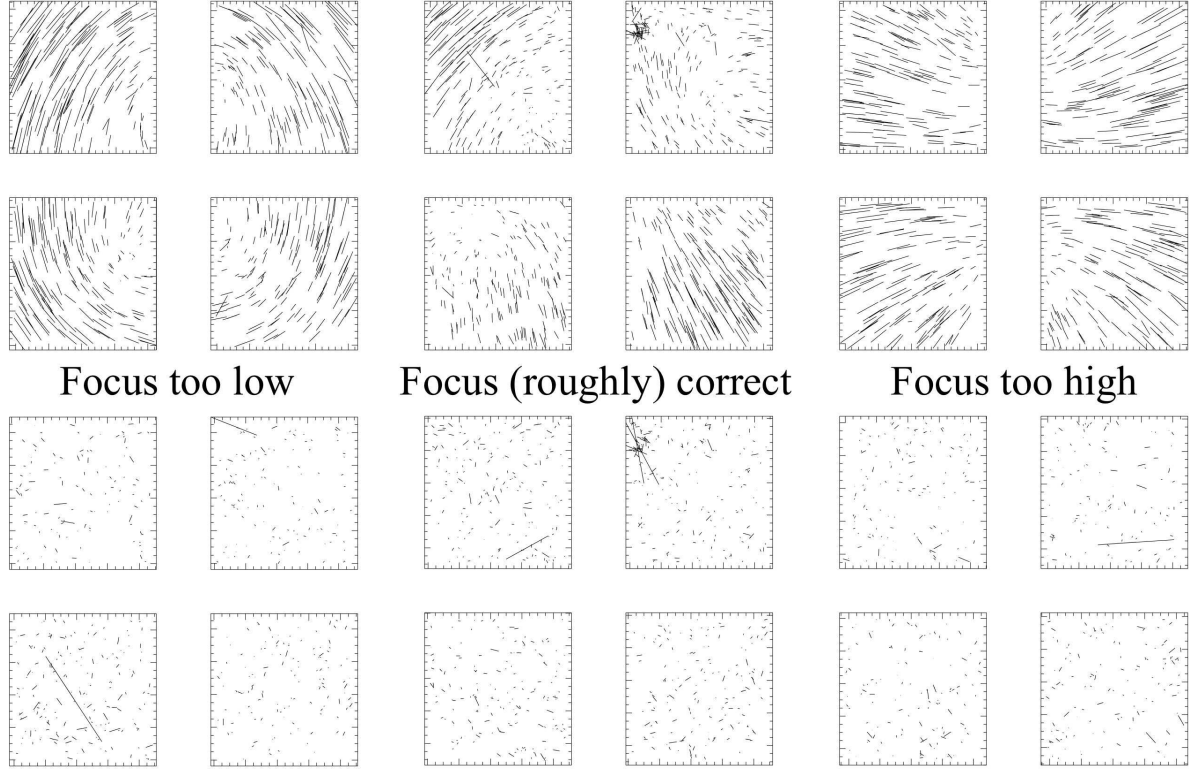


Fig. 1.— Whisker plots of the stars for three of our BTC exposures. The four squares per exposure correspond to the four camera chips, each 15' on a side. In all of the plots, the lengths of the lines are proportional to the ellipticities of the stars, and the orientation is in the same direction as the direction of the ellipticity. The top row show the shapes from the raw images, and the bottom row shows the shapes of the same stars after correction using the PCA technique. The left and right plots represent the two extremes in defocus. The middle is more typical of most of our data.

from some “average” image will not help any image with a different focus value.

3.1. PCA Method

The first step in our PCA technique is to do a polynomial fit of the PSF variation in each image.³ This should be done to a high enough order that the fit describes the bulk properties of the pattern well, but not so high that it gets pulled by noisy measurements. For our data we found that a fourth order fit was adequate.

We arrange these numbers into a matrix M where each row of the matrix corresponds to a different

³Technically, for our analysis, we fit the kernel components, rather than the PSF shape, but as most other lensing analysis techniques do not use deconvolution, we note that the method works exactly the same when fitting the PSF shapes directly.

exposure, and the elements in the row are the numbers from the above fit. Thus for N_{exp} exposures and a fourth order polynomial for each exposure, M is an $N_{\text{exp}} \times 15$ matrix, since there are 15 coefficients in a fourth order polynomial of x, y . We then perform a singular value decomposition of this matrix:

$$M = USV \quad (1)$$

where U and V are unitary matrices, and S is diagonal. The rows of V are called the principal components, and the elements of S are called the singular values. These are in descending order, so that $S(1, 1)$ is the largest singular value.

Each row of M can now be written as a weighted sum of the principal components:

$$M(i, *) = \sum_k U(i, k) S(k, k) V(k, *), \quad (2)$$

where the index i denotes the exposure number. Most of the variation in the rows of M is described by the first principal component ($k = 1$). For our data, since focus seems to be the dominant cause of the variation in our PSF pattern, this coefficient is basically telling us the focus position of that exposure in some arbitrary metric. So we can think of $U(i, 1)$ as the focus position. While the first principal component is indeed fairly dominant, the next several components are not insignificant. The magnitude of each singular value $S(k, k)$ indicates the significance of that component, so one should use the components up to some k_{max} where the singular values become suitably small.

Thus for each star we now have its position, given by x, y , and the above $U(i, k)$ for its exposure. We can now find a global best fit function of these values using the stars in all of our exposures. This will give us a better fit than we had fitting each image individually. The form of this fitting function is somewhat arbitrary. We choose to make a fit which is polynomial in x and y and linear in $U(i, k)$:

$$e_{\text{psf}}(x, y, i) = \sum_k U(i, k) P_k^{(n)}(x, y) \quad (3)$$

where P_k are n th order polynomial functions. We do not need to consider higher order terms in $U(i, k)$, since if the PSF varied as some function of $U(i, 1)$ (for example), instead of linearly, then the singular value decomposition would have picked those values out as the $U(i, 1)$ instead. We also do not include a term with no $U(i, k)$ factor, since to the extent that such a term is important, it will be represented as a linear combination of some of the $U(i, k)$ values.

The real advantage to this fit is that we can now use all of the stars from every image to constrain the fit parameters. There are k_{max} times as many coefficients to constrain, but we have N_{exp} times as many stars to do the constraining. (N_{exp} will generally be at least an order of magnitude larger than k_{max} .)

In addition to providing a better fit in general, it also allows us to take n (the order of the polynomial fits) to be significantly higher than we were able when we were fitting one image at a time. Another advantage is that this technique allows for better outlier rejection, since there is less worry about rejecting all of the stars in a region where the PSF changes quickly, and with more stars to consider, the outliers are more obvious.

Obviously, there are some choices one can make about how many principal components to use (*i.e.* what is k_{\max} ?) and what order to use for the second set of fits (*i.e.* what is n ?). For our analysis, we used up to the principal component whose singular value was 0.01 times the largest singular value, which corresponded to k_{\max} of around 30 for our data. For the BTC data, we chose $n = 10$, and for the Mosaic data, $n = 8$, since the Mosaic PSF patterns were smoother and did not require quite as high a fitting order.

We should point out that using values of k_{\max} and n as high as these is computationally quite demanding. There are k_{\max} n th order polynomials, which have a total of $k_{\max}(n + 1)(n + 2)/2$ coefficients. For our BTC fits, this number is around 2,000. Furthermore, we have 651 BTC exposures, which have a total of almost 100,000 star measurements for each chip. So a least squares fit involves a QR decomposition of a $100,000 \times 2,000$ matrix, which takes of order a day to compute on a desktop computer⁴. The computing time for this step scales as $N_* k_{\max}^2 n^4$, where N_* is the total number of star measurements.

3.2. Prospects for Future Surveys

For future surveys which plan to observe many times the area of the CTIO survey, the number of stars which can be used to constrain the PSF pattern will increase correspondingly. Thus, to the extent that the pattern is really a function of only about k_{\max} parameters, the systematic errors from the PSF fitting will go down as $\sqrt{N_{\exp}}$ along with the statistical errors.

Furthermore, the fits are only accurate down to a scale of $1/n$ times the chip size. For the CTIO data, tenth order fits can correct the correlations down to about $1'$. To accurately correct for the PSF down to $0.5'$ requires doubling n . With more stars, future surveys will have the ability to constrain higher order fits such as this. However, since the computing time for the fits scales as n^4 , such a calculation would take about 16 times as long. So correcting scales much smaller than this would require the use of substantial computing resources.

Note that the description of the $U(i, k)$ values as “focus” values should not be construed to mean that only focus is important. The PCA technique automatically picks out the important effects on the PSF pattern, regardless of the cause, and corrects for them.

For example, ground based telescopes also have systematic errors due to gravity, thermal effects and various other instrumental effects (see Section 4 for a discussion of atmospheric effects). These are likely to have some degree of correlation across exposures, and are generally described by a small number of variables – certainly much smaller than the number of exposures expected in planned surveys.

In space, the principal variation in the PSF will most likely be due to other factors than the focus, since the focus is more stable than for ground-based telescopes. However, even in space the PSF pattern can vary due to effects such as the sun’s relative position, the position in the orbit, periodic mechanical and thermal adjustments or other factors.

⁴Explicit construction of the design matrix takes a similar amount of time.

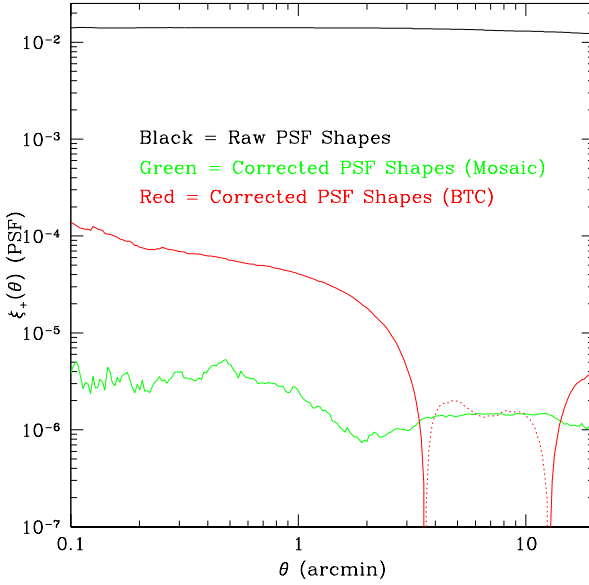


Fig. 2.— The two-point correlation function of the PSF measurements. The upper black curve shows the raw, uncorrected star shapes. The green and red curves show the corrected shapes from the Mosaic and BTC images respectively. The dotted portion of the BTC curve indicates negative values.

One potential improvement to this technique would be to incorporate the idea of Van Waerbeke, Mellier, & Hoekstra (2004) to use rational functions rather than polynomials. They found that rational functions describe the PSF variation better than polynomials, so presumably that would still be the case using our PCA technique. The reason we did not switch to rational functions is that they require a nonlinear fit to determine the parameters. Since we already have very large matrix equations which take quite a while to solve, we did not want to make the calculation take even longer by introducing a nonlinear fit. Also, as our results with polynomials are already consistent with no B-mode, it would be difficult to test for any further improvement. However, we do expect that this change could improve the quality of the fits even further.

3.3. Tests of Effectiveness

The bottom row of Figure 1 show the ellipticities of the stars for three of our BTC images after application of our PCA corrections. The whiskers are not precisely zero, but are consistent with measurement noise. In particular, there are no longer any apparent correlations between the whiskers.

To better test this result, we can measure the two-point correlation function, $\xi_+(\theta)$, for all of the corrected stars in all of the images, limiting to pairs of stars which were observed in the same image. The

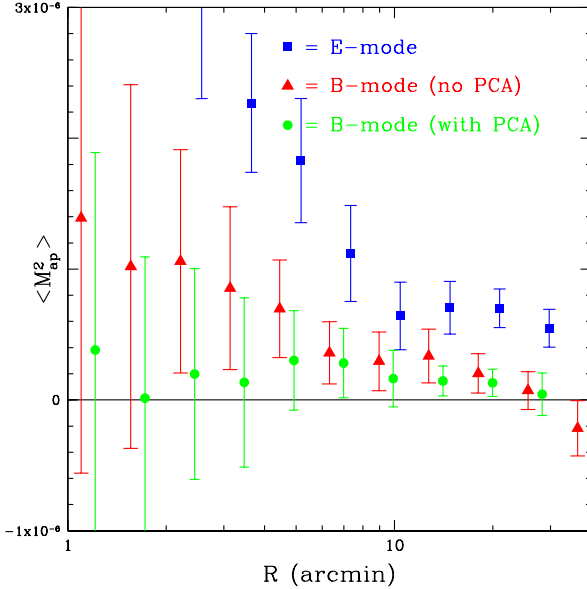


Fig. 3.— The B-mode aperture mass measurements for our CTIO survey data. The triangles and circles are the B-mode with and without using the PCA technique, respectively. The squares are the E-mode measurements.

results of this test are in Figure 2, along with the uncorrected correlation function⁵. For the Mosaic data, the power in the correlation function dropped by almost four orders of magnitude over the entire range from $0.1'$ to $15'$ (the size of the chips). This is remarkable, since the eighth order polynomials were only expected to work well down to about $1'$. This corresponds to a factor of almost 100 reduction in the systematic shape of each star. Furthermore, the effect of this residual on galaxy shapes is smaller still by roughly the ratio of the PSF and galaxy sizes, which is typically about $1/2$ on average.

The results for the BTC data are similar above $3'$, but are somewhat worse below this, where the tenth order fits were apparently insufficient to model the actual patterns. The ringing at higher scales is also indicative that a polynomial is not a very good description of the PSF patterns. It is possible that a different functional form would give better results for these data. However, we note that cameras for future surveys will almost certainly not be as warped as the BTC camera, so the success of the PCA algorithm with the Mosaic data is more relevant for upcoming surveys. For cosmology constraints, we generally limit our consideration to larger scales on which the PSF is well corrected, so the relatively poor corrections at $\theta < 1'$ do not affect the results.

As another test, we can measure the divergence-free B-mode of the shear field for the corrected galaxies. Since weak lensing should only produce a curl-free E-mode signal, a non-zero B-mode indicates the presence of some residual systematic error. One particular statistic which can measure the B-mode is the aperture mass statistic (Schneider *et al.* 1998; Crittenden *et al.* 2002; Schneider, van Waerbeke, & Mellier

⁵Technically, the plotted curve for the raw shapes is for the Mosaic data. The raw BTC curve is very similar, but slightly higher.

2002a; Pen et al. 2002), which has been used quite often for cosmic shear studies. Every weak lensing study which has tested for B-mode has detected some, although usually at a level somewhat less than the E-mode signal and concentrated at smaller scales.

Figure 3 shows the results for our reanalysis⁶. The triangles are the B-mode for fits on a chip-by-chip basis. The circles are the B-mode for fits using the PCA technique. We also plot the E-mode as squares for reference. (The B-mode with no corrections would be off the top of the chart.) The B-mode is now seen to be consistent with zero at nearly all scales, which was not the case for our previous analysis. Our constraints on cosmology using these statistics are presented in Jarvis, Jain & Bernstein (2005).

4. Discussion

We have presented a principal component approach to fitting the PSF anisotropy in imaging data. The stellar PSFs measured in different pointings are combined to obtain a precise estimate of the PSF at the position of each galaxy image. Applying the technique to the CTIO survey data previously presented in Jarvis *et al.* (2003), we find that the measured lensing signal has a much lower systematic contamination. We show two tests: the ellipticity correlation of stars after the PSF correction, and the residual B-mode in the two point correlation of galaxies.

There has been significant recent progress in lensing analysis in all of the critical steps leading to shear estimators: the measurement of galaxy shapes (Kaiser 2000; Bernstein & Jarvis 2002; Refregier 2003; Massey & Refregier 2004), the deconvolution of the PSF to correct the measured shapes (Kaiser 2000; Bernstein & Jarvis 2002; Refregier & Bacon 2003), and the estimation of the PSF at galaxy positions using stellar PSFs (Van Waerbeke, Mellier, & Hoekstra 2004; this work). These developments are important if future lensing surveys are to achieve an accuracy in measurements that is close to the statistical errors. However, there is more work to be done in actually implementing and testing all the pieces that have been presented in the studies cited above.

The principal component approach is applicable to any survey data, since it does not rely on any particular model for the origin of the PSF shape. It simply finds close to the optimal way of using all stellar PSF measurements. We believe it is well suited for the analysis of planned lensing surveys that will cover greater area than ours, such as the Dark Energy⁷, PanSTARRS⁸, LSST⁹, and SNAP¹⁰ surveys. These surveys will have many more pointings than ours, which will enable more accurate fitting of the PSF, since the stacked density of stars is a good indicator of how well the PCA technique can fit the PSF. Statistical

⁶Note that R in Figure 3 is not the same as θ in Figure 2. $R = 1'$ corresponds roughly to $\theta = 2'$.

⁷<http://cosmology.astro.uiuc.edu/DES/>

⁸<http://pan-starrs.ifa.hawaii.edu/>

⁹<http://www.lsst.org/>

¹⁰<http://snap.lbl.gov/>

errors decrease with increasing survey area, and now these surveys can improve their systematic corrections with increasing survey area as well.

We note that if the atmosphere contributes truly random variations with significant power at high spatial frequency, then our technique will not be able to fit for this contribution to the PSF shape. However, such a component is expected to be suppressed for typical weak lensing observations which are taken over 5 minutes or longer. Kaiser, Tonry, & Luppino (2000) estimate the coherence time for the atmosphere’s contribution to the PSF to be of order a second. With exposures which are hundreds of times longer than this, any anisotropic component of the PSF shape from the atmosphere will be highly circularized.

Furthermore, a component of PSF variation that is truly random across exposures is easy to correct with an appropriate survey strategy. In calculating the shear correlation function (from which statistics like the aperture mass described above are derived), one can use only pairs of galaxies that come from different exposures. Then the systematic correlation due to the random component of the PSF variation cannot contaminate the signal. On scales larger than the field of view, this happens automatically. For smaller scales, one needs to observe each location multiple times. This is already common practice to help remove cosmic rays and spurious detections. Using this procedure, the statistical errors would increase by about $\sqrt{N/(N-1)}$ where N is the number of exposures per location, but with modest N , this is a small price to pay to eliminate the remaining systematic errors which the PCA technique cannot remove.

We thank Gary Bernstein for collaborative work on this survey and many helpful discussions. We thank Eric Linder, Masahiro Takada, Ludovic van Waerbeke and Martin White for helpful comments. This work is supported in part by NASA grant NAG5-10924 and by a Keck foundation grant.

REFERENCES

Bacon, D., Massey, R., Refregier, A., & Ellis, R. 2003, MNRAS, 344, 673

Bernstein, G. & Jarvis, M. 2002, AJ, 123, 583

Brown, M., Taylor, A., Bacon, D., Gray, M., Dye, S., Meisenheimer, K., & Wolf, C. 2003, MNRAS, 341, 100

Crittenden, R., Natarajan, P., Pen, U., & Theuns, T. 2002, ApJ, 568, 20

Hamana, T., *et al.* 2003, ApJ, 597, 98

Hirata, C. & Seljak, U. 2003, MNRAS, 343, 459

Hoekstra, H., Franx, M., Kuijken, K., & Squires, G. 1998, ApJ, 504, 636

Hoekstra, H., Yee, H. K. C., & Gladders, M. D. 2002, ApJ, 577, 595

Hoekstra, H. 2004, MNRAS, 347, 1337

Jarvis, M., Bernstein, G., Fischer, P., Smith, D., Jain, B., Tyson, J. A., & Wittman, D. 2003, AJ, 125, 1014

Jarvis, M., Jain, B., & Bernstein, G. 2005, in preparation

Kaiser, N. 2000, ApJ, 537, 555

Kaiser, N., Squires, G., & Broadhurst, T. 1995, ApJ, 449, 460

Kaiser, N., Tonry, J., & Luppino, G. 2000, PASP, 112, 768

Massey, R. & Refregier, A. 2004, MNRAS (submitted, aka astroph/0408445)

Pen, U., van Waerbeke, L., & Mellier, Y. 2002, ApJ, 567, 31

Refregier, A. & Bacon, D. 2003, MNRAS, 338, 48

Refregier, A., Rhodes, J., & Groth, E. J. 2002, ApJ, 572, L131

Refregier, A. 2003, MNRAS, 338, 35

Schneider, P., van Waerbeke, L., Jain, B., & Kruse, G. 1998, MNRAS, 296, 873

Schneider, P., van Waerbeke, L., & Mellier, Y. 2002, A&A, 389, 729

Van Waerbeke, L., Mellier, Y., Pelló, R., Pen, U.-L., McKracken, H. J., & Jain, B. 2002, A&A, 358, 30

Van Waerbeke, L., Mellier, Y., & Hoekstra, H. 2004, A&A (in press, aka astroph/0406468)